REPORT DOCUMENTATION PAGE

Form Approved OMB NO. 0704-0188

1. REPORT DATE (DD-MM-YYYY)	2. REPORT TYPE	3. DATES COVERED (From - To)
01-11-2013	Final Report	5-Aug-2009 - 4-Oct-2013

4. TITLE AND SUBTITLE
Dynamic Pressure Induced Transformation Toughening and Strengthening in Bulk Metallic Glasses

5a. CONTRACT NUMBER
W911NF-09-1-0403

5b. GRANT NUMBER

5c. PROGRAM ELEMENT NUMBER
611102

6. AUTHORS
Jonathon Tooker, Rene Diaz, Alex Bryant, Seung Soon Jang, and Naresh Thadhani

5d. PROJECT NUMBER

5e. TASK NUMBER

5f. WORK UNIT NUMBER

7. PERFORMING ORGANIZATION NAMES AND ADDRESSES
Georgia Tech Research Corporation
Office of Sponsored Programs
505 Tenth Street NW
Atlanta, GA 30332 -0420

8. PERFORMING ORGANIZATION REPORT NUMBER

9. SPONSORING/MONITORING AGENCY NAME(S) AND ADDRESS (ES)
U.S. Army Research Office
P.O. Box 12211
Research Triangle Park, NC 27709-2211

10. SPONSOR/MONITOR'S ACRONYM(S)
ARO

11. SPONSOR/MONITOR'S REPORT NUMBER(S)
56130-MS.1

12. DISTRIBUTION AVAILIBILITY STATEMENT
Approved for Public Release; Distribution Unlimited

13. SUPPLEMENTARY NOTES
The views, opinions and/or findings contained in this report are those of the author(s) and should not contrued as an official Department of the Army position, policy or decision, unless so designated by other documentation.

14. ABSTRACT
The work performed to-date focused on investigation of dynamic pressure induced transformations in simple binary metallic glasses including a Ni80P20 binary alloy in the form of discs cut from an electrodeposited rod made at the Los Alamos National Laboratory, and a Ce75Al25 alloy fabricated via melt spinning at the Ames Laboratory. A Ti-based metallic glass composite was also investigated, in collaborative work with the Jet Propulsion Laboratory, to determine the influence of the in-situ formed crystalline phase on the dynamic compressive and tensile spall strength properties. A number of materials physics and mechanics based fundamental questions were targeted

15. SUBJECT TERMS
bulk metallic glasses; shock compression; phase transformations; crystallization; polyamorphism; shear banding; high-strain-rate deformation

16. SECURITY CLASSIFICATION OF:			17. LIMITATION OF ABSTRACT	15. NUMBER OF PAGES	19a. NAME OF RESPONSIBLE PERSON
a. REPORT	b. ABSTRACT	c. THIS PAGE			Naresh Thadhani
UU	UU	UU	UU		19b. TELEPHONE NUMBER 404-894-2651

Report Title

Dynamic Pressure Induced Transformation Toughening and Strengthening in Bulk Metallic Glasses

ABSTRACT

The work performed to-date focused on investigation of dynamic pressure induced transformations in simple binary metallic glasses including a Ni80P20 binary alloy in the form of discs cut from an electrodeposited rod made at the Los Alamos National Laboratory, and a Ce75Al25 alloy fabricated via melt spinning at the Ames Laboratory. A Ti-based metallic glass composite was also investigated, in collaborative work with the Jet Propulsion Laboratory, to determine the influence of the in-situ formed crystalline phase on the dynamic compressive and tensile spall strength properties. A number of materials physics and mechanics based fundamental questions were targeted, which required an approach that combines the use of time-resolved impact experiments, with continuum- and molecular-scale simulations. With the availability of our 80-mm and 7.63-mm gas-guns, and the laser-accelerated mini-flyer impact set-up, combined with stress, velocity, and imaging diagnostics, we are able to subject materials to uniaxial-stress loading up to 30 GPa and nano-to-micro-second duration, allowing studies of the influence of stress-states and strain-rates on dynamic deformation and phase transformation over a wide range of loading conditions.

Enter List of papers submitted or published that acknowledge ARO support from the start of the project to the date of this printing. List the papers, including journal references, in the following categories:

(a) Papers published in peer-reviewed journals (N/A for none)

Received	Paper

TOTAL:

Number of Papers published in peer-reviewed journals:

(b) Papers published in non-peer-reviewed journals (N/A for none)

Received	Paper

TOTAL:

Number of Papers published in non peer-reviewed journals:

(c) Presentations

Spall and Damage Behavior of Ti-based Intrinsically-Reinforced Bulk Metallic Glass Composites, APS SCCM Topical Group Conference, Seattle, July 8-12, 2013.

Dynamic High Pressure Phase Transformation of Bulk Metallic Glass, AIRAPT-23 International Conference, Mumbai, India, Sep 26-30, 2011

Dynamic Mechanical Behavior of Bulk Metallic Glass and its Composite, TMS Annual Meeting, San Diego, Feb 28, 2011.

Dynamic deformation and pressure-induced transformation in zirconium-based bulk metallic glass, MS&T Conference, Pittsburg, October 2009.

Mechanical Behavior of bulk metallic glass and tungsten composite over a range of strain rates and temperatures, Composites Conference at Lake Louise, October 2009.

Number of Presentations: 5.00

Non Peer-Reviewed Conference Proceeding publications (other than abstracts):

Received	Paper

TOTAL:

Number of Non Peer-Reviewed Conference Proceeding publications (other than abstracts):

Peer-Reviewed Conference Proceeding publications (other than abstracts):

Received	Paper

TOTAL:

Number of Peer-Reviewed Conference Proceeding publications (other than abstracts):

(d) Manuscripts

Received Paper

TOTAL:

Number of Manuscripts:

Books

Received Paper

TOTAL:

Patents Submitted

Patents Awarded

Awards

Rene Diaz, recipient of the 2011 NSF Graduate Research Fellowship

Alex Bryant, recipient of the 2012 NSF Graduate Research Fellowship

Graduate Students

NAME	PERCENT_SUPPORTED	Discipline
Jonathon Tooker	1.00	
Rene Diaz	1.00	
Alex Bryant	1.00	
FTE Equivalent:	**3.00**	
Total Number:	**3**	

Names of Post Doctorates

NAME	PERCENT_SUPPORTED
FTE Equivalent:	
Total Number:	

Names of Faculty Supported

NAME	PERCENT_SUPPORTED	National Academy Member
Seung Soon Jang	0.00	
NAresh Thadhani	0.10	
FTE Equivalent:	**0.10**	
Total Number:	**2**	

Names of Under Graduate students supported

NAME	PERCENT_SUPPORTED	Discipline
Blake Wilkins	0.25	Materials Science & Engineering
FTE Equivalent:	**0.25**	
Total Number:	**1**	

Student Metrics

This section only applies to graduating undergraduates supported by this agreement in this reporting period

The number of undergraduates funded by this agreement who graduated during this period: 0.00

The number of undergraduates funded by this agreement who graduated during this period with a degree in science, mathematics, engineering, or technology fields:..... 0.00

The number of undergraduates funded by your agreement who graduated during this period and will continue to pursue a graduate or Ph.D. degree in science, mathematics, engineering, or technology fields:..... 0.00

Number of graduating undergraduates who achieved a 3.5 GPA to 4.0 (4.0 max scale):..... 0.00

Number of graduating undergraduates funded by a DoD funded Center of Excellence grant for Education, Research and Engineering:..... 0.00

The number of undergraduates funded by your agreement who graduated during this period and intend to work for the Department of Defense 0.00

The number of undergraduates funded by your agreement who graduated during this period and will receive scholarships or fellowships for further studies in science, mathematics, engineering or technology fields:..... 0.00

Names of Personnel receiving masters degrees

NAME
Total Number:

Names of personnel receiving PHDs

NAME
Total Number:

Names of other research staff

NAME	PERCENT_SUPPORTED
FTE Equivalent:	
Total Number:	

Sub Contractors (DD882)

Inventions (DD882)

Scientific Progress

See Attachment

Technology Transfer

Report Title: Dynamic Pressure Induced Transformation Toughening and Strengthening in Bulk Metallic Glasses

Contract No.: W911NF-09-1-0403

Authors: Jonathon Tooker, Rene Diaz, Alex Bryant, Seung Soon Jang, and Naresh Thadhani

ABSTRACT: The work performed to-date focused on investigation of dynamic pressure induced transformations in simple binary metallic glasses including a $Ni_{80}P_{20}$ binary alloy in the form of discs cut from an electrodeposited rod made at the Los Alamos National Laboratory, and a $Ce_{75}Al_{25}$ alloy fabricated via melt spinning at the Ames Laboratory. A Ti-based metallic glass composite was also investigated, in collaborative work with the Jet Propulsion Laboratory, to determine the influence of the in-situ formed crystalline phase on the dynamic compressive and tensile spall strength properties. A number of materials physics and mechanics based fundamental questions were targeted, which required an approach that combines the use of time-resolved impact experiments, with continuum- and molecular-scale simulations. With the availability of our 80-mm and 7.63-mm gas-guns, and the laser-accelerated mini-flyer impact set-up, combined with stress, velocity, and imaging diagnostics, we are able to subject materials to uniaxial-stress loading up to 30 GPa and nano-to-micro-second duration, allowing studies of the influence of stress-states and strain-rates on dynamic deformation and phase transformation over a wide range of loading conditions. The work continues to be performed.

STATEMENT OF PROBLEM: The overall research proposed in this program was aimed at investigating the dynamic pressure induced phase transformation in bulk metallic glasses and its effect on strengthening and toughening under high-strain-rate loading conditions. The program was built on results of our prior ARO-funded work which showed evidence of poly-amorphism in Vitreloy 106 $Zr_{57}Nb_5Cu_{15.4}Ni_{12.6}Al_{10}$ bulk metallic glass (BMG) in which the formation of dense high-pressure amorphous phase of bulk modulus almost 1.5 times higher than the ambient state phase was evidenced[1] based on discontinuities in measured pressure-volume shock compressibility and correlation with the Birch-Murnaghan equation-of-state.[2,3] Anvil-on-rod impact experiments combining time-resolved imaging of transient deformation states and and sample back (free) surface velocity measurements, with continuum-based numerical simulations, also showed that the deformation and failure of the BMG to be well described by the pressure-hardening Drucker-Prager yield and Cumulative Damage failure criteria[4] and substantial increases in yield and fracture stresses, at strain rates in the range of 10^4 to 10^6 s^{-1}. Hence, the current work focused on $Ni_{80}P_{20}$ binary metallic glass alloy discs and a $Ce_{75}Al_{25}$ melt spun alloy, as well as a Ti-based metallic glass composite.

[1] M. Martin, T. Sekine, T. Kobayashi, L. Kecskes, N.N. Thadhani, Metall. Matls. Trans., Vol. 38A, (2007), 2689-96.
[2] F.D. Murnaghan, *Proceedings of the National Academy of Sciences*, vol. 30, pp. 244-247, 1944.
[3] Francis Birch, *Physical Review*, vol. 71, pp. 809-824 (1947).
[4] M.Martin, L. Kecskes, and N.N. Thadhani, Scripta Materialia, 59 (2008), pp. 688-691.

Shock-compression Studies on $Ni_{80}P_{20}$ BMG (Jonathon Tooker)

This project was performed by graduate student Jonathon Tooker who unfortunately left in the middle of the second year of the program.

Experiments using our 80mm single stage gas gun instrumented with photonic Doppler velocimetry (PDV) and polyvinylidene flouride (PVDF) piezoelectric stress gauges were used to determine the U_s-U_p equation of state and P-V compressibility states and infer the occurrence of possible pressure-induced phase transformation in $Ni_{80}P_{20}$. The results of these experiments can be used to verify the predictive capacity of molecular dynamics models. Disc-shaped samples of $Ni_{80}P_{20}$ BMG (density -- 7.77 g/cm3) were obtained from Los Alamos National Laboratories (courtesy of Dr. Ricardo Schwarz). The elastic properties of the amorphous alloy discs were determined using ultrasonic sound speed measurements and are summarized in Table 1.

Table I - Elastic properties of $Ni_{80}P_{20}$ BMG.

Shear wave speed (km/s)	3.932 ± 0.075
Longitudinal wave speed (km/s)	5.442 ± 0.062
Density (g/cm3)	7.77 ± 0.01
Shear modulus (GPa)	120.1 ± 1.80
Elastic modulus (GPa)	229.2 ± 3.43

The pressure-volume compressibility of the BMG was investigated through plate-impact experiments performed using our 80mm single stage gas gun. Figure 1 shows the results based on four symmetric impact experiments performed on the $Ni_{80}P_{20}$ discs. The experiments were instrumented with PVDF piezoelectric stress gauges and PDV impact velocity diagnostics. All U_p and compressed state density values were calculated using the jump conditions, assuming the impedance matching approach. Fig. 1(a) illustrates the behavior of the BMG in the U_s-U_p plane, and Fig. 1 (b) shows the same data plotted in the pressure-density plane. Also included in the plots are the calculated Hugoniots for pure Ni (based on experimental Hugoniot from literature) and amorphous $Ni_{80}P_{20}$ based on measured elastic properties and other constants determined using the Mie-Gruneisen equation of state.

While the number of data points based on the experiments performed are insufficient to determine any trend with respect to phase transition characteristics, the measured compressibility data obtained from the PVDF stress gauge experiments are closer to the calculated Hugoniot for $Ni_{80}P_{20}$ bulk metallic glass than pure crystalline Ni, although the Us-Up relation shows not quite the same fit.

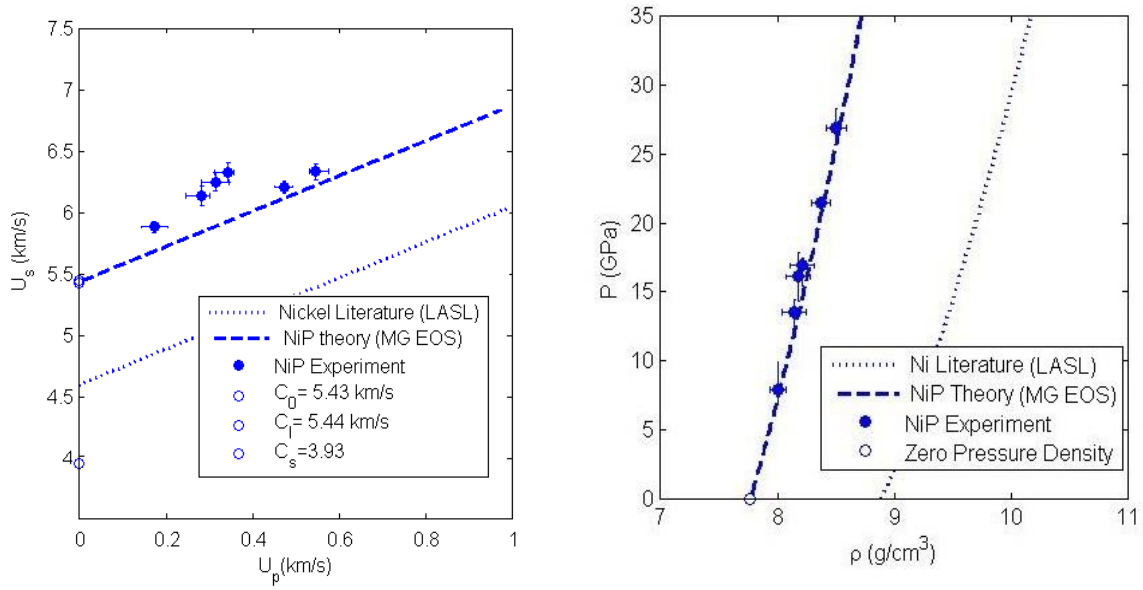

Figure 1: Equation-of-state data plotted in the (a) U_s-U_p plane and (b) pressure-density plane.

Molecular Dynamics studies were also performed in collaboration with Professor Seung Soon Jang in the School of Materials Science at Georgia Tech and with researchers at George Mason University. Using the VASP ab-initio DFT software package, a database of inter-atomic forces was developed over more than 700 hours on a 640 node cluster at George Mason University. The forces were interpolated to build three spline potential functions – each containing thousands of spline knots – approximating the potential energy of nearby Ni and P atoms according to the embedded atom method (EAM). The generic $Ni_{80}P_{20}$ potential needs to be further refined by adding new atomic forces to the spline fitting database generated during DFT simulations specific to the amorphous geometry and $Ni_{80}P_{20}$ stoichiometry of the present BMG. Algorithms for performing uniaxial-stress and uniaxial-strain impact experiments in the LAMMPS MD software framework have been developed and will be employed to simulate meso-scale planar $Ni_{80}P_{20}$ impact experiments.

The results of these simulations remain to be verified using the data generated by the experiments performed in this research. The experimental-computational feedback is expected to lead to a predictive capability for the Hugoniot behavior $Ni_{80}P_{20}$, in order to obtain realistic determination of phase transformation characteristics and its mechanisms.

Shock-compression Studies on $Ce_{75}Al_{25}$ Metallic Glass Ribbons (Alex Bryant)

This project is being performed by graduate student Alex Bryant who is currently a second year student, and a recipient of the NSF Graduate Research Fellowship.

Recent studies employing static high pressure work at APS have shown $Ce_{75}Al_{25}$ metallic glass undergoing transformation from the amorphous state at ambient conditions to FCC crystalline state at 25 GPa.[5] [5.3.182]. $Ce_{75}Al_{25}$ is an interesting metallic glass as it possibly contains a random mixture of the elements. Pure Ce and Al have an fcc structure and upon solidification often produce preferred orientation. At ambient pressure, Ce has an atomic volume twice that of Al, but a lower electronegativity. Because of this extreme mismatch between the two atoms, solidification of the alloy from the melt results in the formation of a glass, which however shares the common long-range topological relationship with the fcc crystal, albeit without its long-range spatial periodicity, consistent with the cluster packing model typical of glasses.[6] Upon being compressed, the atomic volume of Ce collapses due to the delocalization of the 4f electrons, which reduces the differences between the compressed Ce and Al and results in the Hume-Rothery criteria for crystallization of fcc solid solution. Pressure-induced devitrification then restores the hidden long-range through transformation into a single crystal.

In the present work, $Ce_{75}Al_{25}$ metallic glass ribbons made via melt spinning were obtained from Ames Laboratory. The as-received ribbons of 40 μm thickness had opposite surfaces with a matte and reflective finishes, with the matte finish corresponding to the surface in contact with the melt spinning wheel, and the reflective surface exposed to the environment. XRD analysis of the respective surfaces confirmed (as shown in Figure 2), that the reflective side had a partially crystalline oxide surface coating, closely matching with Ce_6O_{11}, and the matte side, however, was clearly amorphous. The matte side surface corresponds to the melt being solidified in contact with the water-cooled copper wheel, resulting in the fastest cooling rate ensuring the amorphous state and replicating the surface texture of the copper wheel on the ribbon. The reflective side, exposed to the environment, albeit vacuum, has an oxide coating due to reaction with the trace amounts of oxygen present and partial crystallization due to somewhat slower solidification rate.

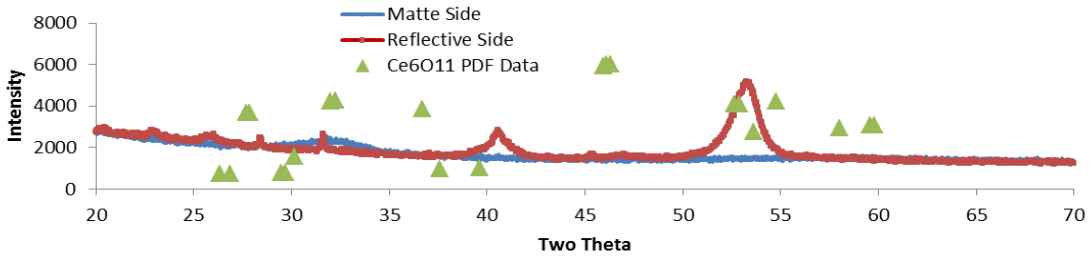

Figure 1 shows the different XRD results for the two sides. The matte side is clearly amorphous while the reflective side has a crystallinity that matches the peaks for CeO.

[5] Q. Zeng, *et al*. Science 332, 1404 (2011).
[6] D. B. Miracle, JOM, Vol. 64, No. 7 (2012).

High-resolution imaging using the Hitachi SU8010 Cold Field Emission SEM with a BSE detector, showed evidence of dendrite formation in some areas on the reflective surface of the ribbons. As shown in figure 3, the dendrites are on the order of less than 100 nm in size and need to be further characterized via TEM analysis to determine the depth of the partially crystalline regions.

Figure 3 shows dendritic growths observed at high magnifications of 25,000X and 50,000X in the CeAl ribbon on the MG side. White square lines indicate areas that were heated extensively by long periods of exposure to the electron beam.

SEM images of cross-sections edges of scissor-cut ribbons are shown in Figure 4. Although the formation of a lip impedes clear observation, it appears that the crystalline areas may be isolated in various (top) regions of the melt-spun ribbons.

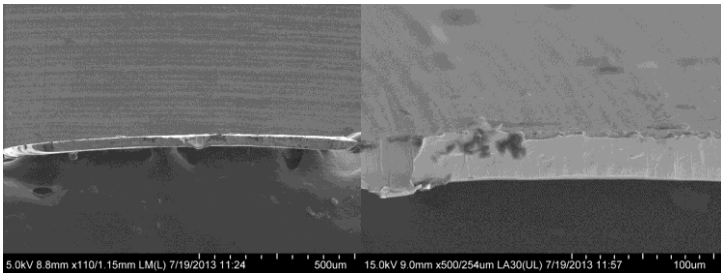

Figure 4. SEM images of cross-sectional edges of scissor-cut ribbons showing isolated crystalline (dark) regions at top.

Density measurements performed with the Archimedes method, employing a surface tension lowering liquid added to water and using a long ribbon piece, yielded a value of 5.93 g/cm^3 for the $Ce_{75}Al_{25}$ metallic glass ribbon, which is lower than the calculated density (6.21 g/cm^3) for the crystalline alloy obtained using the rule of mixtures. Table II compares physical properties of $Ce_{75}Al_{25}$ metallic glass with that of crystalline state, Ce, Al, and quartz.

Table II - Physical properties of $Ce_{75}Al_{25}$ metallic glass as compared with those of crystalline alloy, Al, Ce, and quartz.

Material	Density	Sound Speed	Impedance
$Ce_{75}Al_{25}$ crystalline (calculated RoM)	6.21	1.55	9.63
$Ce_{75}Al_{25}$ met. glass	5.93	1.55	9.19
Cerium	6.77	1.18	7.99
Aluminum	2.70	5.35	14.46
Quartz (z-axis)	2.65	6.36	16.85
LiF	2.64	5.2	13.73

The metallic glass ribbons were also characterized via Local Electrode Atom Probe (LEAP) using the facilities at the Oak Ridge National Laboratory. Preliminary results were limited due to time constraints and the depth of penetration/analysis. Nevertheless, it was found that there were clusters of 80 atomic% Ce throughout the as-received sample, as seen in figure 5. However, it is not obvious if these clusters are either nearly pure Ce or $Ce_{75}Al_{25}$. A proposal for in-depth characterization has been submitted to ORNL to obtain further time on the LEAP, and thereby gather detailed information on the atomic composition variations throughout the ribbons.

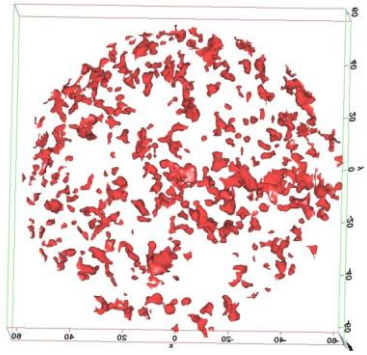

Figure 5. LEAP results showing isoconcentration profile of clusters of 80 atomic%Ce in as-received $Ce_{75}Al_{25}$ melt-spun ribbon.

Laser Shock Experiments

Considering the small thickness of the $Ce_{75}Al_{25}$ melt-spun ribbons, shock compression experiments cannot be performed using traditional gas-gun type loading geometries. We are therefore collaborating with Bruce Remington and his group at the Lawrence Livermore National Laboratory, for direct laser shock experiments using the Omega, Janus, and NIF laser facilities. A series of experiments have been performed during two separate campaigns.

Rochester #1, February 2013: Two 1mm x 1mm samples of $Ce_{75}Al_{25}$ melt-spun ribbons were placed into laser sample recovery tubes and brought to the Omega Laser Facility at the Laboratory for Laser Energetics (LLE) in Rochester, NY, for shots performed at 20J and 80J, respectively, in order to characterize the dynamic response at pressures slightly lower and higher than reported the 25 GPa hydrostatic pressure that resulted in instant and complete devitrification of $Ce_{75}Al_{25}$ in prior work. The expected pressure was calculated using Hyades. The recovered samples are awaiting XRD and TEM analysis.

Rochester #2, August 2013: Four additional recovery tube-enclosed sample stacks of ~70 ribbons (each 1mm x 2mm x 40um) were prepared at Georgia Tech, and sent to the Omega facility. The samples were shot at 70J and 150J, with Hyades calculations showing large attenuation from the layers of sample. Stacks were hit either into the face of the stack or into the edge of the stack so as to observe the different shock characteristics and characterize the different radial distribution of the shock energy effects in the two orientations. The edge on sample also ensured the laser would hit a relevant portion with less worry about errors in the adjustment. The recovered samples are awaiting XRD and TEM analysis.

Molecular Dynamics Simulations

Graduate student Alex Bryant has also been learning how to use Cerius2, a molecular dynamics program and LAMMPS, a powerful discrete particle simulator. Along with running basic simulations on copper crystals that are about 120 nm^3 to determine their stability at room temperature, he also simulated amorphous $Ce_{75}Al_{25}$, utilizing randomized placement of atoms in the right atomic ratio and allowing them to stabilize with time at room temperature and ambient pressure. Figure 6 shows the instability of 120 nm^3 of amorphous copper, and the relative stability of the amorphous structure of the $Ce_{75}Al_{25}$ metallic glass at ambient conditions. Since the $Ce_{75}Al_{25}$ simulations utilized a potential derived from many *ab initio* simulations, they are expected to be correct. A potential for the high pressure state of the system is also available, which has been provided by Professor Howard Sheng at George Mason University. We will be collaborating with him in order to better understand the creation of potentials as well as for the creation of our empirical potential that will allow us to transition from amorphous to crystalline as needed to match what we will be observing from our experiments. From this empirical potential and these experimental observations, we expect to be able to better understand how the 4f electron delocalization works temporally as well as spatially, in order to explain the expected difference in effects from shock loading versus hydrostatic pressure.

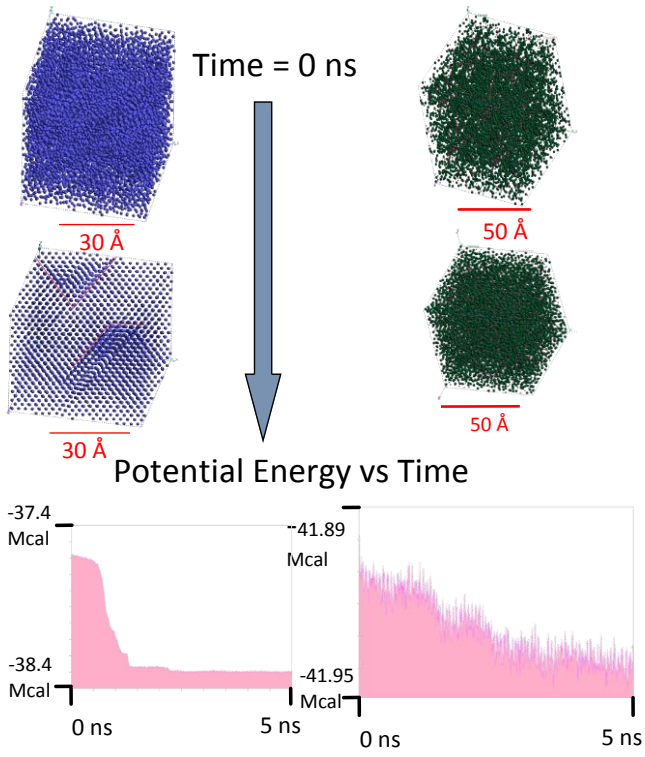

Figure 6. Visualizations depicting changing atomic structure of initially amorphous Cu (left) and $Ce_{75}Al25$ (right) at ambient conditions over the course of 5ns. The interaction energies' progressions with time are shown in plots for Cu (left) and Ce75Al25 (right).

This work focusing on both experimental and computational aspects will continue over the next couple of years as part of Alex Bryant's dissertation research.

Spall and Damage Behavior of Ti-Based DVI metal glass matrix composites (Rene Diaz)

This project is being performed by graduate student Rene Diaz who is currently a third year student, and a recipient of the NSF Graduate Research Fellowship.

While bulk metallic glasses are potential next-generation structural materials with applications in many industries because of their near theoretical yield strength, high elastic strain limit, carbide-like hardness, corrosion resistance, and thermoplastic processability,[7] bulk metallic glass matrix composites (BMGMCs) have been found to impart critical reinforcement properties to overcome brittle failure in tension. BMGMCs contain crystalline dendritic inclusions which act to stabilize the glass against unlimited shear band extension and enable global plasticity and graceful failure under opening stress. Specifically, it has been demonstrated that the length scales associated with size and distribution of dendrites has a profound effect on mechanical properties such as ductility, fracture toughness, and fatigue endurance.

Uniaxial-strain plate-impact experiments were performed to study the dynamic compressive strength and spall damage of bulk metallic glass-matrix composites (BMGMCs). BMGMCs counteract the brittle nature of monolithic BMGs through *in-situ* formed crystalline dendrites which increases toughness and ductility. Applications for shielding against micrometeorites, kinetic energy penetrators (KEP), and armor, raise the question of the dynamic stability of BMGMCs. The multicomponent Ti-based BMGMCs were investigated in this work using uniaxial-strain plate-impact experiments to examine the phase stability of the dendrite-reinforced BMGMCs under high pressure and their high strain-rate deformation and failure response. The experiments involved impact of 303 stainless steel flyer-plate on 303 stainless steel sample holder containing two BMGMC samples, at varying velocities. The Hugoniot Elastic Limit (HEL) and the spall strength of the BMGMC samples were determined using velocity interferometry system for any reflector (VISAR). Post-mortem microstructural characterization was done the on the recovered sample and correlated with the measured damage response.

The BMGMC alloy investigated was DV1 $Ti_{44.3}Zr_{35.2}V_{11.8}Cu_{6.1}Be_{2.6}$ (wt%) and $Ti_{48}Zr_{20}V_{12}Cu_5Be_{15}$ (at%). The advantage of utilizing a Ti-based over existing Zr-based BMGMCs is the reduction in cost and density.[8,9,10] The DV1 BMGMC alloy was provided by NASA's Jet Propulsion Laboratory and tested in the as-received condition. Table III lists the static mechanical and acoustic properties of the DV1 alloy. Quantitative stereological analysis was conducted on the as-received samples to determine the volume fraction of dendrites (V_v), surface-to-volume ratio (S_v), and dendrite arm spacing ($\Omega = 4\left[\frac{1-V_v}{S_v}\right]$), which are also listed in Table III.

[7] W. L. Johnson, MRS Bull. 24, 42 (1999).
[8] D. C. Hofmann, J-Y. Suh, A. Wiest, G. Duan, M-L. Lind, M. D. Demetriou and W. L. Johnson, Nature 451, 1085 (2008) and Scr. Mater. 59, 684 (2008).
[9] M. Davidson, S.Roberts, G. Castro, R.P. Dillon, A.Kunz, H. Kozachkov, M.D. Demetriou, W. L. Johnson, S. Nutt and D. C. Hofmann, Advanced Engineering Materials 15, 27 (2013).
[10] M.M.Trexler and N. N. Thadhani, Progress in Materials Science 55, 759 (2010).

Table 3. Static mechanical properties of Ti-based DV1 BMCMC as compared to those of crystalline titanium of commercial purity and its alloys.

Name	wt%	BMG, %	BCC, %	ρ, g/cm^3	σ_y, MPa	σ_{Max}, MPa	ε_y, %	ε_{tot}, %	σ_{Max}/ρ, MPa•cm^3/g	RoA, %	K_{1C}, MPa•m$^{1/2}$	E, GPa	G, GPa	ν	T_s, K
DV1	$Ti_{44}Zr_{35.2}V_{11.8}Cu_{6.1}Be_{2.6}$	53	47	5.15	1362	1429	2.3	12.5	277	43	43.8	94.2	34.4	0.368	955
Ti-6-4a	$Ti_{90}Al_6V_4$ (grade 5 annealed)	N/A	N/A	4.43	754	882	1	16.4	199	42	100	113.8	44	0.342	1877
Ti-6-4 s	$Ti_{90}Al_6V_4$ (grade 5 STA)	N/A	N/A	4.43	1170	1170	~1	~10	264	N/A	43	114	44	0.33	1877
CP-Ti	Ti_{100} (grade 2)	N/A	N/A	4.51	409	409	0.7	25.5	91	46	66	105	45	0.37	~1930

Back-scattered scanning electron microscopy using an Amray 1810 SEM revealed spatially-dependent dendrite morphology with two dendritic "phases" α-Primary dendrites and β-secondary dendrites as shown in Figure 7. Due to the identical contrast from the back-scatter imaging, the primary and secondary dendrites appear to be compositionally identical. The primary dendrites constitute a volume fraction (V_v^{α}) of 0.3989 ± 0.02292, a surface-to-volume ratio (S_v^{α}) of 38.74 ± 0.00093 mm^2/mm^3, and dendrite arm spacing of 0.0621 mm.

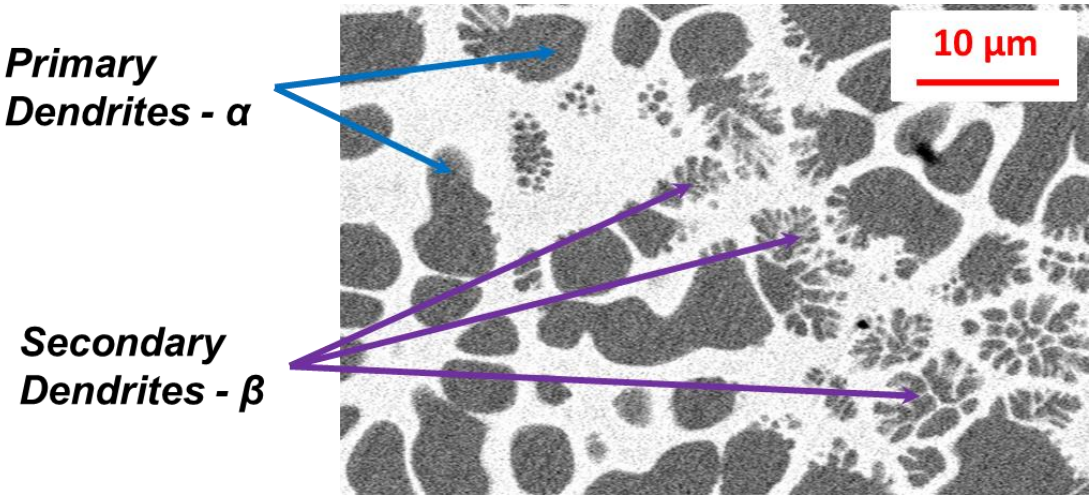

Figure 7. DV1 alloy dendrite morphology showing secondary dendrites nucleating from the primary dendrites in the as-cast alloy

Sound speed measurements were performed using an Olympus 5072PR pulse/receiver in the pulse echo configuration attached to both Ultran VSP-200 and SRD50-5 ultrasonic probes for longitudinal and shear wave velocity measurements respectively. The data were recorded using a Tektronix DPO 5104 1 GHz oscilloscope. The longitudinal, shear, and bulk sound speeds (C_L, C_s, and C_B, respectively) are given in Table IV. Density was measured using Archimedes method.

Table IV Density and sound speed properties of DV1. C_L – Longitudinal sound speed, C_S – shear sound speed, C_B – Bulk Sound speed ($C_B = \sqrt{C_L^2 - \frac{4}{3}C_S^2}$), and ρ_0 – initial density.

	C_L (mm/μs)	C_S (mm/μs)	C_B (mm/μs)	ρ_0 (g/cm^3)
DV1	5.337 ± 0.0996	2.489 ± 0.0475	4.4976 ± 0.0007	5.194 ± 0.005

Uniaxial-strain plate-impact experiments were conducted using the 80 mm diameter single-stage gas-gun at the Georgia Institute of Technology. An aluminum sabot was used as the projectile with 303 Stainless Steel (SS) flyer plate to impact the DV1 bulk metallic glass composite. As shown in the schematic in Figure 8, the flyer plate was backed with a hollow backer (air gap) to allow generation of release waves in the flyer plate. The samples were machined with a 10° taper designed to break free from the holder upon impact. The target DV1 plate was twice the thickness of the flyer plate in order to allow the release waves from the rear surfaces of the target and flyer plates to coalesce on the mid-plane of the target plate. The coalescence of release waves generates tension and consequent spallation.[11] The sample holder was mounted onto a poly(methy methacrylate) (PMMA) ring. Behind the PMMA target ring, a rigid polycarbonate plate was used with an opening large enough to allow the samples to pass through for subsequent soft-recovery, while preventing the surrounding target ring and projectile following the sample and inducing secondary impact. The samples were recovered in the catch tank behind the chamber in a bed of soft rags.

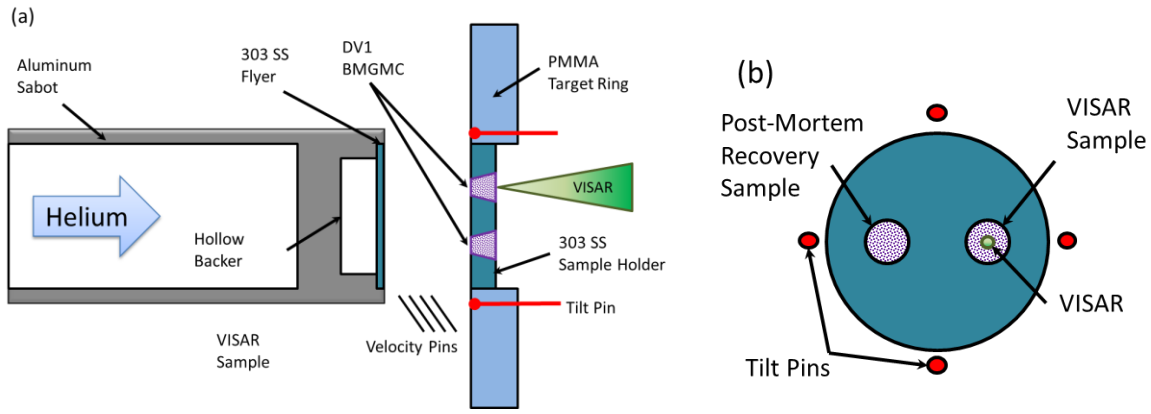

Figure 8. Schematic of set-up used for plate-impact experiments performed on DV1 BMGMC

[11] RL Whelchel, GB Kennedy, SK Dwivedi, TH Sanders Jr and NN Thadhani, J. Appl. Phys. 113, 233506 (2013).

Impact velocity was determined utilizing four velocity pins at fixed locations in which their separation distance was measured using a depth micrometer. The time between each pin being triggered was used to calculate the average impact velocity. The actual tilt between the two plates was measured by recording the times at which four isolated voltage-biased pins, flush with the surface of the target plate, were shorted to the ground. The multi-beam VALYN™ VISAR velocity interferometer was used to measure the history of the normal particle velocity at the rear surface of the target plate. Figure 9 illustrates the VISAR traces obtained from the various experiments. The traces illustrate clear indication of the Hugoniot elastic limit (in the rise to peak pressure state) and the spall (pull-back) signal. It can be seen that the shock compressed state in the DV1 alloy is attained through the propagation of an elastic wave of amplitude between 5.7 to 6.7 GPa with the final state attained through the propagation of a slower shock wave.

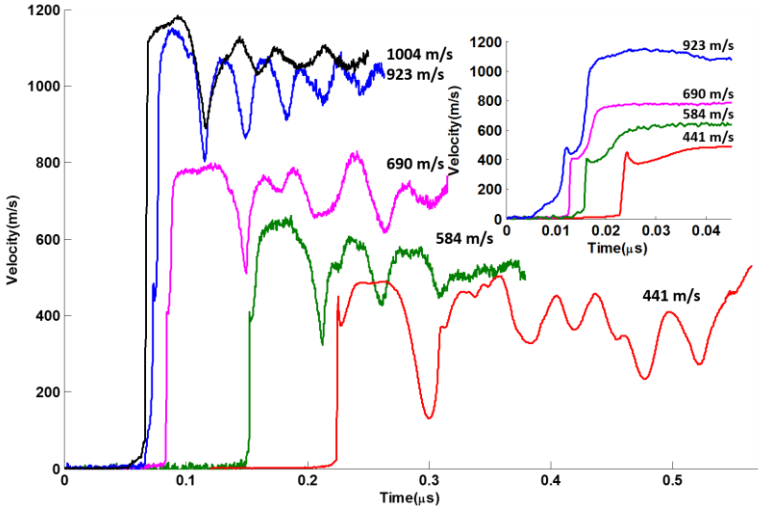

Figure 9. VISAR traces obtained from various experiments performed on DV1 $Ti_{44.3}Zr_{35.2}V_{11.8}Cu_{6.1}Be_{2.6}$ metallic glass composite samples.

Dandekar and Spletzer[12] have observed a similar decay in the amplitude of the elastic precursor but with a significantly lower HEL (2-3 GPa), in Ti-6Al-4V. The slower shock wave has the signature of plastic wave propagation. While the velocity profile correlates closer to DV1's crystalline counterpart, Ti-6Al-4V, the HEL range is closer to that of monolithic Zr-based BMGs. Experiments conducted on Vit 106 ($Zr_{58.5}Cu_{15.3}Ni_{12.8}Al_{10.3}Nb_{2.8}$) by Trexler *et al.*[10] yielded an average HEL of 6.86 GPa. Gupta *et al.*[13] performed similar shock wave experiments on $Zr_{56.7}Cu_{15.3}Ni_{12.5}Nb_5Al_{10}Y_{0.5}$ and found an HEL of 7.1 ± 0.3 GPa and Mashimo *et al.*[14] observed an HEL of 6.2 GPa in $Zr_{55}Al_{10}Ni_5Cu_{30}$. It is important to note that a similar decay in amplitude or "dip" in HEL is seen with the monolithic Zr-based BMGs right after the HEL but is attributed to its elasto-isotropic solid, in which shear strength is catastrophically lost above the HEL. However, the loss of shear strength is associated with formation of shear bands, the primary form of failure in monolithic metallic glasses. Due to the presence of the crystalline dendrites in DV1, shear band formation in metallic glass matrix is arrested. Under static conditions, this is evidenced by the serrated nature of the tension curve just before failure. Each drop in stress is

[12] D. P. Dandekar, and S. V. Spletzer, Shock Response of Ti-6Al-4V, 2000), p. 427.
[13] S. J. Turneaure, J. Winey, and Y. Gupta, Appl. Phys. Lett. 84, 10 (2004).
[14] T. Mashimo, H. Togo, Y. Zhang, Y. Uemura, T. Kinoshita, M. Kodama, and Y. Kawamura, Appl. Phys. Lett. 89, 24 (2006).

associated with a normally catastrophic shear band being arrested by the microstructure, leading to significant necking (43% reduction in area).

Equations (1)–(2)[11] were used to determine the Hugoniot Elastic Limit (σ_{HEL}) and spall strength (σ_{spall}). Measured material parameters include the density (ρ_0), longitudinal sound speed (C_L), and bulk sound speed (C_B). Data measured during plate impact testing includes the free surface velocity at the HEL (u_{HEL}), the change in free surface velocity from the peak to the pullback minimum (Δu_{fs}), and the slopes of the free surface velocity before and after the pullback minimum (velocities u_1 and u_2 respectively). The calculated values of the Hugoniot Elastic Limit (σ_{HEL}) and the spall strength (σ_{spall}), along with the peak stress and the experimental conditions are listed in Table V.

$$\sigma_{HEL} = \frac{1}{2}\rho_0 C_L u_{HEL} \quad (1)$$

$$\sigma_{spall} = \frac{1}{2}\rho_0 C_B (\Delta u_{fs} + \delta) \quad (2)$$

Table V lists the parameters for the various experiments.

Velocity (m/s)	Flyer Plate thickness (mm)	Sample Thickness (mm)	Fringe constant (m/s)	Fringes Added	Spall Strength (GPa)	Hugoniot Elastic Limit (GPa)	Peak Stress (GPa)
441.5 ± 3.18	1.386	2.194	99.4	3	4.1 ± 0.04	6.2 ± 0.97	5.5 ± 0.22
584.1 ± 16.15	1.334	1.828	874	0	3.6 ± 0.01	5.7 ± 0.7	8.4 ± 0.12
689.6 ± 12.88	1.427	1.828	874	0	3.2 ± 0.01	5.7 ± 0.7	10.6 ± 0.15
923.9 ± 40.45	0.902	1.824	874	0	3.3 ± 0.02	6.7 ± 0.7	14.4 ± 0.36
1003.9 ± 47.99	1.351	1.606	330.9	3	2.9 ± 0.08	N/A	N/A

Figure 10 compares the spall strength as a function of the impact stress of the DV1 composite glass in comparison to monolithic Zr-based metallic glasses that have undergone shock experiments. The DV1 alloy is found to have a slower rate of decay in spall strength and a higher spall overall strength (~4 GPa) than the monolithic Zr-based BMGs, in which case the spall strength decreases at a much faster rate with increasing impact stress.

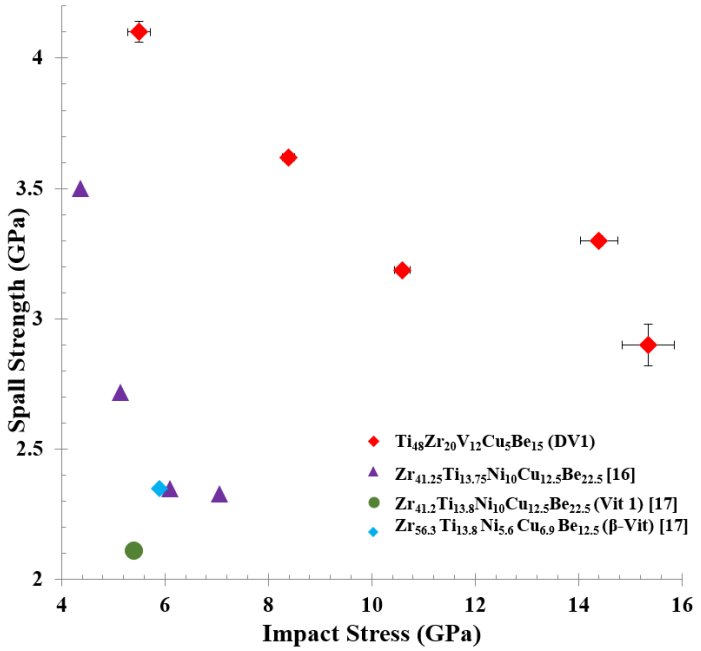

Figure 10. Spall strength plotted as a function of impact stress for DV1 ($Ti_{44.3}Zr_{35.2}V_{11.8}Cu_{6.1}Be_{2.6}$) alloy in comparison to three different Zr-based BMGs.

The recovered impacted samples were also characterized via electron microscopy to observe the fracture path and the influence on the in-situ formed dendrites on fracture mitigation. Figure 11 shows optical micrographs from the experiment performed at 441 m/s in which case the sample did not spall completely, as is also evident in the free-surface velocity trace with its significant pull-back signal (in Figure 9). As a result, the spall fracture path shows a partial characteristic "saw-tooth" pattern. The crack propagated crushing through the soft dendrite in through "inter-dendritic" fracture.

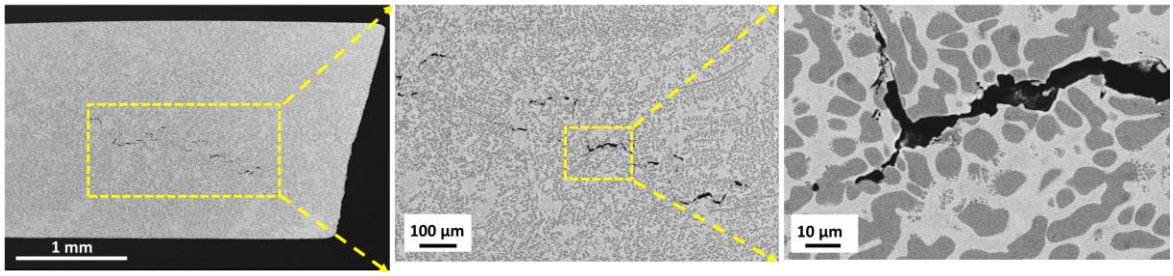

Figure 11. Micrographs revealing fracture path in DV1 sample impacted at 440 m/s

The primary mode of fracture seems to be occurring from microvoid coalescence nucleating and growing in the dendrites (Fig 12a). This mode of fracture is associated with ductile spallation seen in metals as opposed to microcracking, a brittle fracture mechanism. Evidence of ductile failure is further evidenced by the presence of a dimpled fracture surface as revealed in the topographical SEM image (Fig. 12b), which also shows presence of microvoids. The dendrites being the softer phase appear to act as strain concentrators and become the

precursors to crack formation in the otherwise stiffer metallic glass matrix. This is the opposite scenario as what has been observed with Vitreloy-106 bulk metallic matrix composite with tungsten particle reinforcement, which restrict propagation of shear bands forming in the glassy matrix.[10]

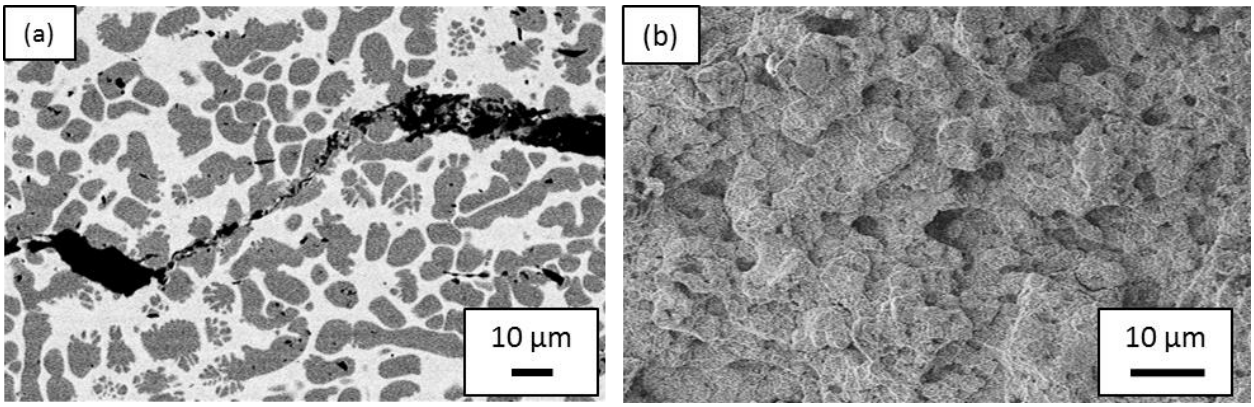

Figure 12 (a) Microvoid nucleation and coalescence in dendrites and (b) microvoids forming in ductile dendritic region.

In summary, the uniaxial-strain plate impact experiments performed on DV1 ($Ti_{44.3}Zr_{35.2}V_{11.8}Cu_{6.1}Be_{2.6}$) BMGMC using VISAR velocity interferometry reveal clear evidence of characteristics of the Hugoniot Elastic Limit and spall pull-back signals. Post-mortem fractography revealed dendrites behaving as precursors to crack formation through nucleation and coalescence of microvoids within the dendrites. Microvoids were present in the dimple fracture region or ductile region along the spall plane.

This work focusing on both experimental and computational aspects will continue over the next couple of years as part of Rene Diaz's dissertation research.